

OPEN ACCESS

EDITED BY James Scott Maki, Marquette University, United States

REVIEWED BY
Jean-Philippe Belliard,
University of Antwerp, Belgium
Hai-Hoa Nguyen,
Vietnam National University of Forestry,
Vietnam

*CORRESPONDENCE
Yongze Xing
Xingyongze@4io.org.cn

RECEIVED 10 May 2025 ACCEPTED 15 September 2025 PUBLISHED 29 September 2025

CITATION

Zhao L, Chen D, Tan H, Wang Y, Qiao Y and Xing Y (2025) The response of mangrove degradation to mineral composition. *Front. Mar. Sci.* 12:1626088. doi: 10.3389/fmars.2025.1626088

COPYRIGHT

© 2025 Zhao, Chen, Tan, Wang, Qiao and Xing. This is an open-access article distributed under the terms of the Creative Commons Attribution License (CC BY). The use, distribution or reproduction in other forums is permitted, provided the original author(s) and the copyright owner(s) are credited and that the original publication in this journal is cited, in accordance with accepted academic practice. No use, distribution or reproduction is permitted which does not comply with these terms.

The response of mangrove degradation to mineral composition

Lintao Zhao^{1,2,3}, Dezhi Chen^{1,2,3}, Haoyuan Tan^{1,2,3}, Yingjing Wang^{1,2,3}, Ying Qiao^{1,2,3} and Yongze Xing^{1,2,3}*

¹Key Laboratory of Tropical Marine Ecosystem and Bioresource, Fourth Institute of Oceanography, Ministry of Natural Resources, Beihai, China, ²Guangxi Key Laboratory of Beibu Gulf Marine Resources, Environment and Sustainable Development, Fourth Institute of Oceanography, Ministry of Natural Resources, Beihai, China, ³Observation and Research Station of Coastal Wetland Ecosystem in Beibu Gulf. Ministry of Natural Resources. Beihai, China

Mangrove wetlands serve as pivotal ecotones at land-sea interfaces, where habitat stability is critically modulated by sediment mineralogical composition. However, the impacts of anthropogenic activities on mineralogical evolution and associated ecological consequences in these ecosystems remain poorly understood. This study examines these processes in a degraded mangrove ecosystem within Tieshangang Bay, China, to uncover engineering-induced perturbations and their implications for mangrove health. Integrated mineralogical analyses were employed, including X-ray diffraction (XRD) and automated mineralogical parameter analysis (MapsMin), to characterize sediment composition and discern anthropogenic influences. These techniques enabled high-resolution quantification of mineral distributions and associations across degraded and preserved zones. The results reveal pronounced kaolinite enrichment (48.97-66.35%) in surficial sediments (0-15 cm) of degraded zones, contrasting with stable mineralogical composition in preserved areas. Diagnostic mineral assemblages and spatial patterns implicate terrestrial clay inputs from port infrastructure expansion and dredging operations, exacerbated by tidal channel obstruction and hydrodynamic attenuation. Mechanistic analysis demonstrates that kaolinite's platy morphology promotes pore occlusion, reducing sediment porosity and inducing rootzone hypoxia, which drives mangrove regression. Based on these findings, a synergistic remediation framework is proposed, integrating tidal hydrology restoration, sediment source regulation, and substrate permeability enhancement. These insights advance the understanding of anthropogenicgeochemical-ecological cascades in intertidal ecosystems and provide a mineralogical benchmark for nature-based mangrove conservation and coastal resilience management.

KEYWORDS

kaolinite, mineral composition, mangrove, human activities, Beibu Gulf

1 Introduction

Mangroves, as woody plant communities endemic to tropical-subtropical intertidal zones, originated along the Tethyan Ocean margins during the Late Cretaceous to Paleogene (Ellison et al., 1999), with extant species comprising 73 true mangrove taxa and hybrids (Spalding et al., 2010). These high-productivity ecosystems exhibit net primary productivity of 1,500–3,500 g C·m⁺²·yr⁺¹, rivaling biomass accumulation rates of tropical rainforests and coral reef systems (Alongi, 2014). Globally distributed across 150,000 km² of sheltered coastlines within 20° latitude of the equator, mangroves predominantly occupy Atlantic, Indian, and Pacific marginal seas (Temmerman et al., 2013; Bunting et al., 2022a). In China, their northern distribution limit extends to Zhejiang (28°N), with major concentrations in Guangdong, Guangxi, Hainan, Fujian, and the Greater Bay Area (Liao and Zhang, 2014; Zhang et al., 2021).

Functioning as critical ecotonal components, mangroves mediate coastal purification through root filtration and sediment adsorption, leveraging unique biogeochemical processes to immobilize heavy metals (bioaccumulation factors: 10²–10³ for Cd/Pb) and sequester nutrients (>70% N/P removal efficiency), effectively mitigating nearshore eutrophication (Usman et al., 2013; Chaudhuri et al., 2014; Souza et al., 2015; Rezaei et al., 2021). This bioshield capacity positions mangroves as nature-based solutions for coastal pollution remediation.

As key sedimentary archives in land-sea transition zones, mangrove habitats operate under coupled terrestrial-marine forcings, representing Earth's most dynamic interfaces for matterenergy fluxes. Their spatial distribution and ecological functions are governed by multiscale drivers: natural factors including substrate composition, hydrothermal regimes (mean annual temperature/ precipitation), hydrodynamic processes (tides/waves/currents), geomorphology (shoreline slope), seawater chemistry (salinity/ pH), and global change stressors (sea-level rise/elevated CO₂) (Liao and Zhang, 2014; Gilman et al., 2008); anthropogenic pressures encompass aquaculture expansion, agricultural nonpoint pollution, coastal urbanization, and industrial effluents (UNEP, 2014). Despite their irreplaceable roles in carbon sequestration, biodiversity conservation, and shoreline protection, mangroves remain among Earth's most threatened ecosystems, with global annual loss rates of 0.16-0.39% during 2000-2012, particularly acute in Southeast Asia due to intensive coastal development (Hamilton and Casey, 2016; Goldberg et al., 2020; Bunting et al., 2022b).

The Beibu Gulf coast, a global hotspot for mangrove research (Xia, 2011), exemplifies the tension between ecological preservation and maritime economic growth. Degradation episodes observed in Beihai's Tieshangang Harbor underscore the urgency for reconciling resource exploitation with ecosystem integrity. Systematic characterization of mangrove environmental baselines and evolutionary trajectories thus forms the scientific foundation for sustainable governance.

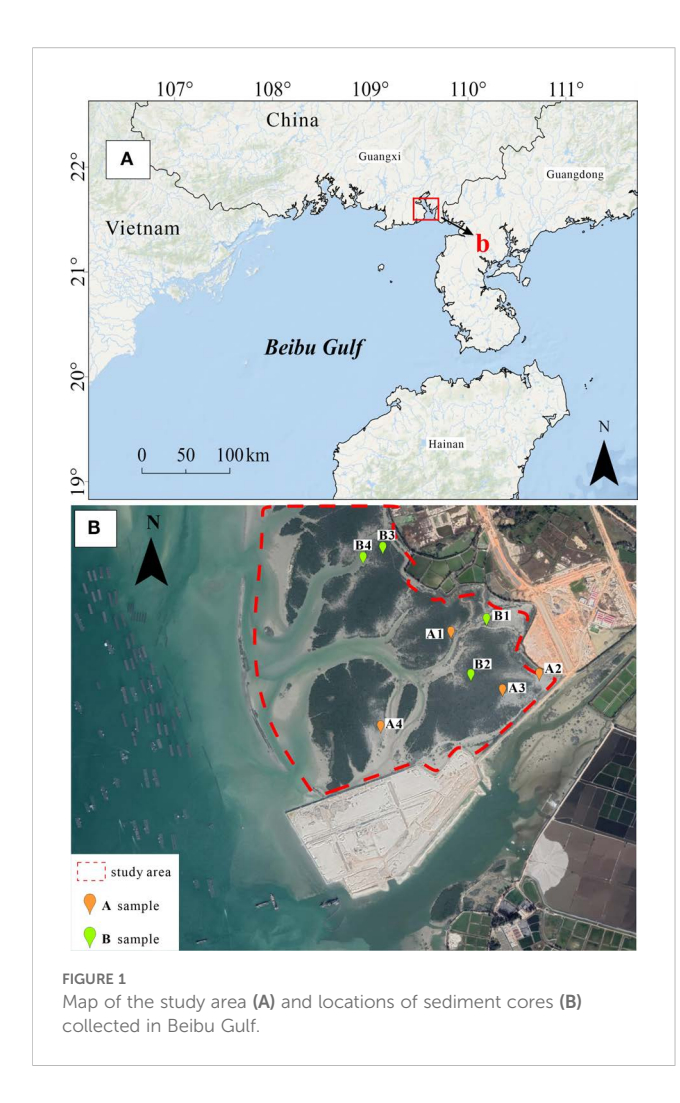
Sediments, as central vectors in material cycling (Meng et al., 2006), encode both regional geochemical signatures and

anthropogenic pollutant trajectories. Mangrove sediments, formed through the long-term development of mangrove ecosystems, represent a distinct soil type whose genesis is intrinsically linked to tidal dynamics, sediment properties, and vegetation characteristics (Xia, 2015). These sediments are typically composed of silt and clay deposited by riverine and coastal processes. Sediment texture exhibits significant spatial variation contingent upon local hydrology and sediment provenance. Estuarine mangrove sediments, receiving substantial terrestrial and marine inputs, are characterized by finer particles and elevated organic matter content. In contrast, marine mangrove sediments, more isolated from fluvial sources, contain coarser particles and lower organic matter concentrations (Zhang et al., 2024; Grellier et al., 2017). The pneumatophores and prop roots of mangrove trees, in conjunction with bioturbation by benthic fauna, create intricate networks of pores and voids within the sediment matrix, significantly enhancing soil aeration and structural stability (Numbere and Obanye, 2023; Xia, 2015). Mineralogical analysis of depositional records enables spatiotemporal reconstruction of landwater-biota interactions, unraveling coupled natural-anthropogenic drivers to inform coastal management. This study employs X-ray diffraction (XRD) and automated mineral parameter analysis (MapsMin) to investigate sediment mineral assemblages in Tieshangang's degraded mangrove wetlands (Figure 1). We aim to: (1) elucidate engineering-induced mineralogical shifts across disturbance gradients; (2) decipher mineral-environment feedbacks governing mangrove decline; (3) provides effective mitigation strategies for mangrove degradation induced by elevated clay mineral content, delivering theoretical foundations and technical pathways for ecological risk assessment of coastal engineering and mangrove wetland restoration.

2 Materials and methods

2.1 Study area

Tieshangang Bay, a semi-enclosed basin elongated meridionally in the northeastern Beibu Gulf, spans a 170 km coastline and encompasses 340 km² of aquatic domain. This geomorphologically privileged system combines extensive tidal prism dynamics (tidal range reaching 5 m), favorable bathymetric conditions (maximum depth >20 m), and low-wave-energy regimes, synergized with abundant hinterland resources, positioning it as a strategic deepwater port development zone in southwestern China. The research area is situated within Beihai City's predominant industrial cluster, hosting established facilities for photovoltaic production, mineral processing, and pulp and paper manufacturing. A series of port infrastructures have been developed along both shores of the embayment, with ongoing expansion projects to enhance its role as a regional maritime logistics hub. Extensive typical mangrove communities thrive across the intertidal zones flanking Tieshangang Bay, forming critical ecological barriers. Dominant species include Avicennia marina, Aegiceras corniculatum, and Rhizophora stylosa. Canopy heights are generally below 3.5 m,



predominantly ranging from 2–3 m, with a mean diameter at breast height (DBH) of 12 cm. Notable growth disparities were observed among mangrove stands: while some sectors exhibit vigorous development, others display stunted growth accompanied by mortality events affecting both saplings and mature trees. Comparative analysis of Landsat imagery (pre-construction [2017] vs. post-construction [2021]) revealed a marked NDVI reduction in the eastern study area during 2021, field-verified through ground observations. This decline prompted investigation into its causal attribution (Figure 2).

2.2 Field sampling

In this study, the sample collection was not conducted strictly following a linear sampling method; rather, it was based on random sampling triggered by observing situations where mangrove plants were thriving or exhibiting distinct mortality during the field investigation. Sampling sites were stratified by vegetation vigor: areas exhibiting robust mangrove growth were classified as degraded (Area A, n = 4), while areas displaying partial mortality of both saplings and mature trees were designated preserved (Area B, n = 4). A total of 8 sediment cores (50 cm in length) were collected from these

areas(Figure 1), and the elevation at each sampling location was measured (Table 1). Core collection employed a modified peat corer to ensure intact stratigraphic sequences, with vertical subsampling guided by a density-optimized protocol: surface sediments (0–20 cm depth) were sectioned at 5 cm intervals, transitioning to 10 cm intervals below 20 cm. All samples were immediately sealed in sterile polyethylene bags, stored at 4°C in lightproof containers, and transported under chain-of-custody protocols to minimize biogeochemical alterations prior to laboratory analysis.

2.3 Analytical methods

2.3.1 XRD

X-ray diffraction (XRD) analyses were conducted at Northwest University following standardized mineralogical protocols (Wang et al., 2021). Sample preparation involved sequential pretreatment steps: (1) manual removal of allochthonous materials (shell fragments, plant debris); (2) desiccation to constant mass in a temperature-controlled oven (45°C); (3) particle size reduction to <75 µm (200 mesh) using an agate mortar. Mineralogical characterization was performed using a Bruker D8 Advance diffractometer equipped with Cu K α radiation ($\lambda = 0.15406$ nm), Lynxeye_XE-T detector (2.9472° divergence angle), and 2.5° Soller slits. Operational parameters were optimized as: 40 kV tube voltage, 40 mA current, 3-25° 2θ scanning range, 0.02° step size, 0.6 s/step counting time, and 0.6 mm incident slit width. Analytical reproducibility was ensured through rigorous adherence to quartz internal standard calibration and triplicate measurements of representative samples.

2.3.2 MapsMin

Automated mineralogical analyses were systematically conducted at Thermo Fisher Scientific (Guangzhou, China) on selected 0–5 cm layer of the A4 core sample. Sample preparation involved epoxy resin impregnation of bulk sediments, followed by mechano-chemical polishing to achieve optical-grade planar surfaces. To mitigate scanning electron microscopy (SEM) charging artifacts and enhance signal-to-noise ratios, a homogeneous conductive carbon coating (~10 nm thickness) was deposited via magnetron sputtering. Processed mounts were analyzed using an Apreo field-emission SEM equipped with MapsMin automated mineralogy software, operating under high-vacuum conditions (<10⁺³ Pa).

The MapsMin workflow comprised four stages:

Navigational Imaging: Global backscattered electron (BSE) mosaics (5 μ m pixel⁺¹ resolution) were acquired via automated stage mapping to delineate regions of interest.

Target Selection: Statistically representative areas (≥10% of total surface) were identified through iterative thresholding of BSE grayscale histograms (8-bit depth) and energy-dispersive spectroscopy (EDS) prescan mineralogical screening.

High-Resolution Mapping: Selected zones were algorithmically subdivided into $500\times500~\mu m$ to $2\times2~mm$ tiles for pixel-wise analysis, with acquisition parameters dynamically optimized:



BSE imaging: 0.05-1 µm pixel⁺¹, 1-3 µs dwell time;

EDS spectral collection: $0.5-2~\mu m$ step size, 4-10~ms dwell time; Phase Identification: Mineralogical classification was executed through spectral library matching ($\geq 95\%$ confidence threshold) against a bespoke database containing 1,200+ verified mineral phases.

3 Results

3.1 Sedimentary stratigraphy

Core stratigraphy reveals pronounced chromatic differentiation correlated with organic-clay mineral interactions, delineating depositional environment gradients:

TABLE 1 Sampling points location information.

Sample	Coordinates		Elevation (m)
A1	109°36′48.55″E	21°35′47.80″N	-16.39
A2	109°37′05.67″E	21°35′40.58″N	-15.67
A3	109°36′58.62″E	21°35′37.36″N	-15.79
A4	109°36′35.41″E	21°35′30.40″N	-16.30
B1	109°36′55.63″E	21°35′50.54″N	-16.31
B2	109°36′52.07″E	21°35′39.79″N	-16.08
В3	109°36′35.80″E	21°36′04.34″N	-16.41
B4	109°36′32.98″E	21°36′03.26″N	-16.74

Degraded zones (A1-A4):

Surficial lithofacies (0-15 cm): Grayish-white horizons exhibit elevated clay mineral content, indicative of anomalous terrigenous clay influx.

Subsurface transition (15–50 cm): Gradational darkening to gray-black hues reflects humic acid-clay complexes, diagnostic of sustained sulfate-reducing regimes.

Preserved zones (B1-B4):

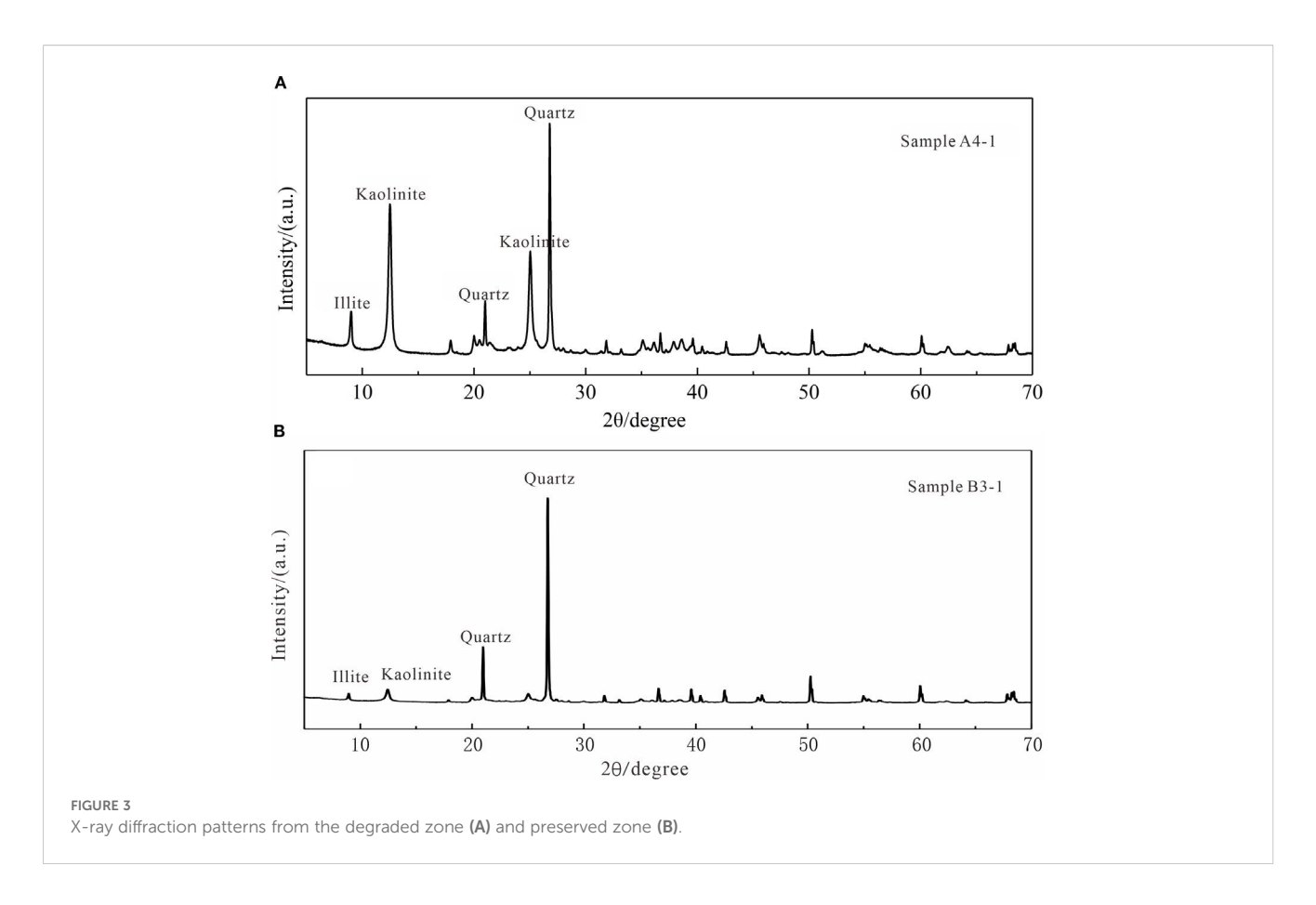
Surficial lithofacies (0–15 cm): Light grayish-white sediments exhibit minimal clay mineral variance, indicating negligible terrigenous clay input.

Subsurface transition (15–50 cm): Progressive chromatic transition to gray-black matrices incorporates discrete reddish-brown laminations. These features represent humic substance accumulation—specifically fulvic acid and humic acid generated by anaerobic diagenesis of mangrove detritus.

The data reveal a marked disparity in surficial kaolinite content (0–15 cm depth) between degraded and preserved zones. Degraded zones exhibit kaolinite concentrations of 37.45–66.35% (mean: 56.90%), contrasting sharply with preserved zones at 13.05–33.92% (mean: 24.51%). This pronounced spatial heterogeneity necessitates further investigation into localized drivers of kaolinite distribution.

3.2 Mineral assemblage characteristics

This study conducted mineralogical analysis on sediment cores from both degraded (Zone A) and preserved (Zone B) mangrove wetlands, examining the vertical distribution characteristics of minerals across eight cores (A1-A4, B1-B4). X-ray diffraction



(XRD) data reveal that the sedimentary matrix is predominantly composed of quartz, kaolinite, and illite, with significant spatiotemporal differentiation in mineral abundances across sampling stations and vertical stratigraphy(Figure 3, Table 2).

To address limitations in XRD detection thresholds for trace mineral phases (<2 wt%), supplementary Maps Mineralogy analyses were implemented. Results confirm the dominance of kaolinite-quartz-illite assemblages while identifying a secondary mineral suite comprising (Figure 4):

Silicates: Plagioclase, muscovite, K-feldspar, biotite, zircon, chlorite;

Phosphates/Carbonates: Apatite, monazite, calcite, siderite, dolomite-ankerite;

Sulfides/Oxides: Pyrite, gypsum/anhydrite, rutile, ilmenite.

3.3 The spatial distribution characteristics of minerals

Automated mineralogical mapping reveals distinct spatialpartitioning patterns across the Tieshangang mangrove wetlands, with vertical and lateral heterogeneity governed by depositional regimes (Figure 5).

1. In the degraded area (Area A), the core samples show a typical pattern of high kaolinite enrichment in the surface layer and rapid attenuation in the middle layer:

Kaolinite characteristics: A significant enrichment layer (48.97% - 66.35%) is formed in the surface 0–15 cm, with a content as high as 66.35% in A3 core sample 0–5 cm. With the increase in depth, the kaolinite content shows an exponential attenuation trend. The content in the 15–20 cm layer of A1 core sample decreased by 62.3% (from 45.68% to 17.21%). Notably, A2 - A4 core samples still maintained a content of > 30% below 20 cm, while the content in the 20 cm below of A1 core sample dropped sharply to < 15%.

Quartz characteristics: As the dominant detrital mineral, quartz content shows strong fluctuation (22.98% - 76.20%), with low content in the shallow layer and high content in the deep layer. A1 core sample shows an extreme high value (76.20%), indicating enhanced terrestrial input in this area.

Illite characteristics: The content is relatively stable (6.64% - 20.95%), with small fluctuations with depth. Among them, the illite content in A1 core sample is significantly higher (12.54% - 20.95%) compared among the four cores in the damaged area.

2. In the preserved area (Area B), the mineral composition shows a slow changing distribution pattern:

Kaolinite characteristics: The enrichment degree in the surface layer is significantly lower than that in the degraded area (25.21% - 33.92%), and the vertical attenuation is gentle. The content in the 0–5 cm layer of B1 core sample is 33.92%, and it still maintains 13.80% in the 15–20 cm layer. B2 core sample shows a sub-surface enrichment phenomenon, with a content of 30.33% in the 10–15 cm layer.

TABLE 2 Mineral composition information of sediment samples.

Mineral content(%) Depth Sample (cm) Quartz Kaolinite A 1-1 0-5 33 37 45.68 20.95 A1-2 5-10 42.45 20.89 36.66 A1-3 10-15 42.27 37.45 20.28 A1-4 15-20 67.29 17.21 15.50 A1-5 20-30 73.89 12.11 13.99 A1-6 30-40 76.20 11.27 12.54 A1-7 40-50 70.75 14.33 14.92 A2-1 0-5 24.96 65.35 9.69 A2-2 5-10 22.98 65.25 11.76 10.81 A2-3 10-15 23.59 65.60 A2-4 15-20 37 11 49 28 13.61 20-30 43.43 40.69 15.88 A2-5 31.27 A2-6 30-40 56.13 12.60 40-50 30.75 A2-7 58.14 11.11 A3-1 0-5 24.40 66.35 9.25 A3-2 5-10 23.61 65.56 10.83 48.97 A3-3 10-15 37.95 13.08 A3-4 15-20 49.63 38.88 11.49 A3-5 20-30 50.54 38.08 11.38 A3-6 30-40 49.01 39.40 11.59 A3-7 40-50 65.83 25.54 8.63 A4-1 0-5 26.56 64.83 8.62 A4-2 5-10 27.28 63.75 8 98 A4-3 10-15 39 27 51 53 9.21 10.73 A4-4 15-20 46.61 42.65 29.53 A4-5 20-30 62.39 8.08 A4-6 30-40 60.91 30.85 8.24 A4-7 40-50 63.99 29.37 6.64 B1-1 0-5 59.90 33.92 6.17 B1-2 5-10 76.53 17.36 6.10 B1-3 10-15 84.15 10.76 5.09 B1-4 15-20 79.08 13.80 7.13 B1-5 20-30 74.13 19.43 6.44 B1-6 30-40 63.85 26.91 9.24 B1-7 40-50 68.60 25.04 6.36 B2-1 67 74 26 49 5 77 0-5 B2-2 27.86 5-10 66.00 6.13

(Continued)

TABLE 2 Continued

Sample	Depth	Mineral content(%)		
	(cm)	Quartz	Kaolinite	Illite
B2-3	10-15	61.36	30.33	8.32
B2-4	15-20	68.29	25.46	6.25
B2-5	20-30	67.62	24.37	8.01
B2-6	30-40	72.90	20.18	6.92
B2-7	40-50	68.84	23.72	7.43
B3-1	0-5	62.34	29.52	8.14
B3-2	5-10	60.90	29.22	9.89
B3-3	10-15	62.01	28.65	9.33
B3-4	15-20	64.99	26.27	8.75
B3-5	20-30	67.86	23.74	8.40
B3-6	30-40	73.12	18.12	8.76
B3-7	40-50	70.04	19.41	10.55
B4-1	0-5	68.34	25.21	6.44
B4-2	5-10	71.03	21.71	7.26
B4-3	10-15	79.90	13.05	7.05
B4-4	15-20	82.82	12.36	4.82
B4-5	20-30	83.12	11.48	5.39
B4-6	30-40	80.84	12.42	6.74
B4-7	40-50	76.81	11.09	12.10

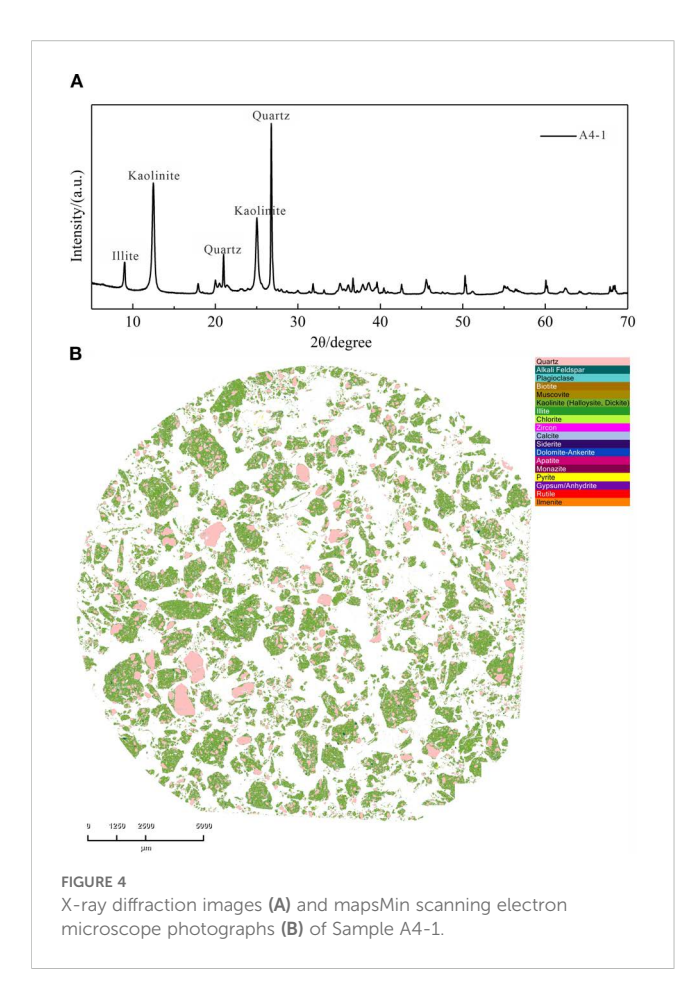
Quartz dominance: As the main mineral component, quartz content is generally higher than that in the degraded area (59.90% - 83.12%), with a content as high as 83.12% in B4 core sample.

Illite characteristics: The content range is 4.82% - 12.10%, with no obvious vertical change trend. B3 core sample shows a typical box-shaped distribution (8.14% - 10.55%), reflecting a stable sedimentary environment.

4 Discussion

4.1 Provenance of kaolinite

The Tieshan Bay area is tectonically situated within the Beibu Gulf Depression of the South China Fold System. Through a series of plate tectonic processes including rifting, subduction, convergence, and collision, multiple magmatic events occurred in the study area, forming magmatic rocks of Caledonian, Indosinian, and Yanshanian ages (Zhao et al., 2023). Caledonian magmatic rocks are predominantly composed of granitic gneiss and granodiorite (Qin et al., 2006). The Indosinian magmatism is represented by the Shiwandashan-Liuwandashan-Darongshan batholith, mainly consisting of cordierite-bearing granites (Zhang et al., 2017). Yanshanian magmatic rocks, though small in scale but



widely distributed, include biotite granite, quartz monzonite, and monzogranite (Li et al., 2000). These widespread granitoids provided abundant source materials for kaolinite formation. Under warm-humid climatic conditions, granitoids underwent rainwater leaching that removed alkaline ions, leaving behind silica and alumina to form kaolinite, which was subsequently transported and deposited in the bay by surface runoff. Analytical data from this study reveal that mangrove sediments contain quartz, kaolinite, illite, K-feldspar, plagioclase, zircon, topaz, tourmaline, apatite, monazite, pyrite, rutile, boehmite, and biotite. These minerals predominantly represent residual or weathering products of granitoids, further confirming that the coastal sediments in Tieshangang are derived from weathering of northern granitoids in the study area.

4.2 Causes of shallow kaolinite enrichment

Comparative analysis of the degraded zone (Area A) and preserved zone (Area B) reveals a significant enrichment of kaolinite in surface sediments of Area A. The kaolinite content in Area B exhibits minimal stratigraphic variation, representing baseline depositional conditions for regional kaolinite. Integrated analysis of environmental perturbations suggests three primary mechanisms driving shallow kaolinite enrichment in Area A:

4.2.1 Anthropogenic infrastructure development

Satellite imagery from 2017 (Figure 6A) documents pristine mangrove ecosystems with minimal adjacent development. Contrastingly, 2021 imagery (Figure 6B) reveals extensive coastal modifications including port facilities, dredged material disposal sites, and terrestrial engineering projects along the eastern, northern, and western peripheries. Proximal to eastern construction zones (subareas A2-A4), unmitigated sediment mobilization from exposed construction materials facilitated rapid kaolinite accumulation through tidal/pluvial transport. Subarea A1 demonstrates enhanced kaolinite retention due to its low-lying topography creating a hydrologic trap for suspended particulates.

4.2.2 Navigation channel maintenance

Chronic sediment input from fluvial systems necessitates recurrent dredging to maintain navigable depths. The absence of sediment containment measures during dredge operations resuspends channel-bottom deposits, particularly kaolinite-rich clays, into the water column. Subsequent tidal advection transports these fine particulates into mangrove ecosystems where flocculation and deposition occur.

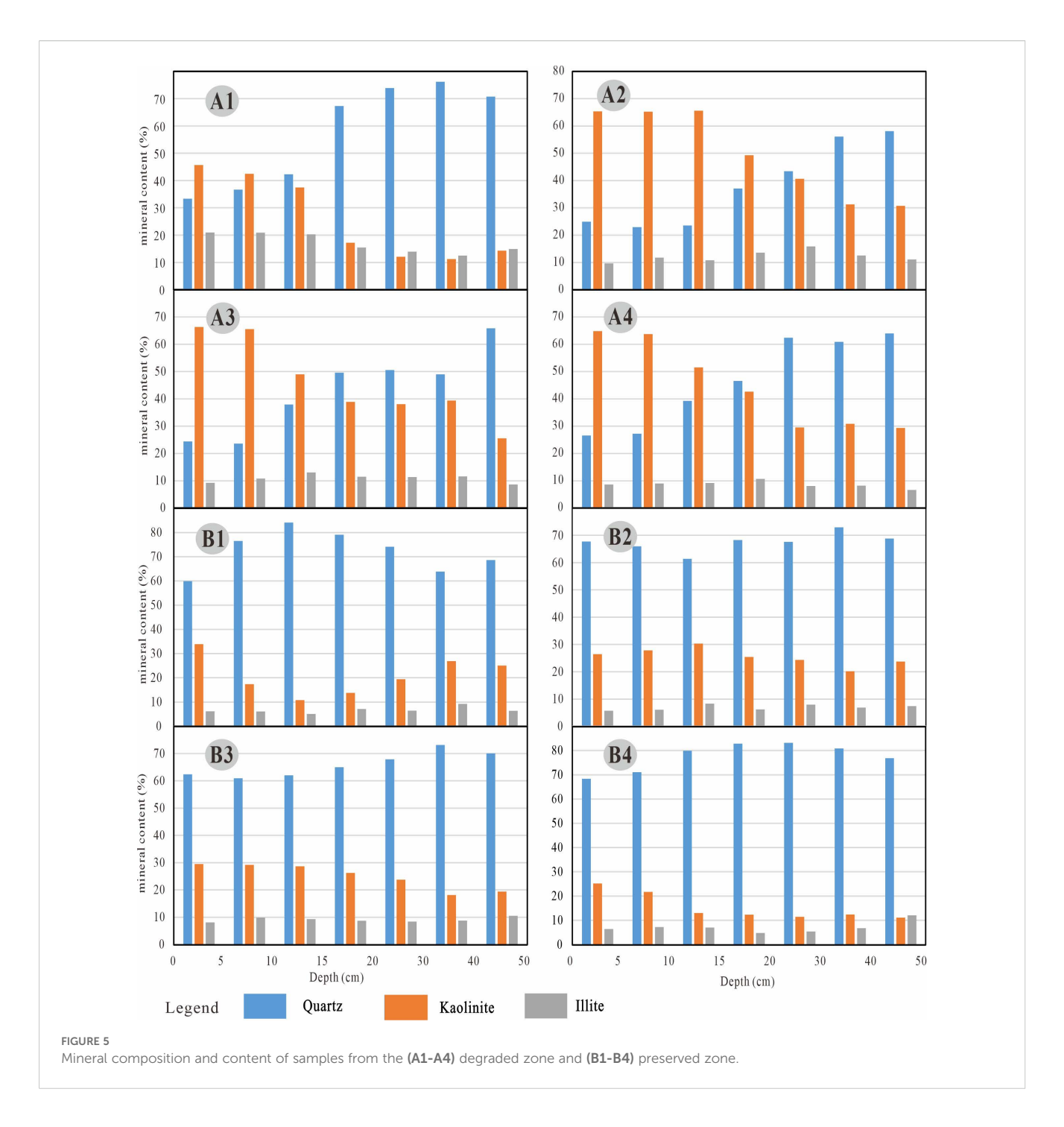
4.2.3 Tidal hydrodynamic attenuation

Tieshangang Bay constitutes a large semi-enclosed embayment in the northwestern Beibu Gulf. Its tidal hydrodynamics exhibit distinct characteristics modulated by astronomical tides, wind forcing, bathymetric constraints, and anthropogenic interventions. The system experiences a predominantly diurnal tidal regime featuring single flood-ebb cycles daily, though with noted irregularities in tidal range and phase. Tidal currents demonstrate canonical diurnal reversals, alternating between flood- and ebb-dominant phases over semi-diurnal intervals. 2017 imagery (Figure 6a) illustrates an intact tidal network with multiple southern/western channels enabling efficient marine flushing. By 2021 (Figure 6b), critical southern channels had been replaced by port infrastructure, restricting connectivity to two diminished northwestern conduits. This geomorphic alteration reduced tidal prism volume by ~65%, decreasing current velocities from 0.8-1.2 m/s to 0.3-0.5 m/s. The resultant shift from high-energy tidal regimes to low-energy lagoonal conditions (evidenced by increased water residence time from <12 hr to >36 hr) fundamentally altered sediment dynamics. Reduced hydrodynamic competence impaired both landward sediment transport during flood tides and seaward export during ebb phases, creating net depositional conditions for anthropogenicallysourced kaolinite.

4.2.4 Non-mineralogical contributing factors

Integrated analysis indicates that mangrove degradation involves factors beyond the three primary drivers, including altitude gradients (Table 1), microrelief configurations, soil drainage capacity, and sediment granulometry. Comparative assessment reveals:

Preserved Zones (B1, B3, B4): Higher elevation proximal to terrestrial margins.

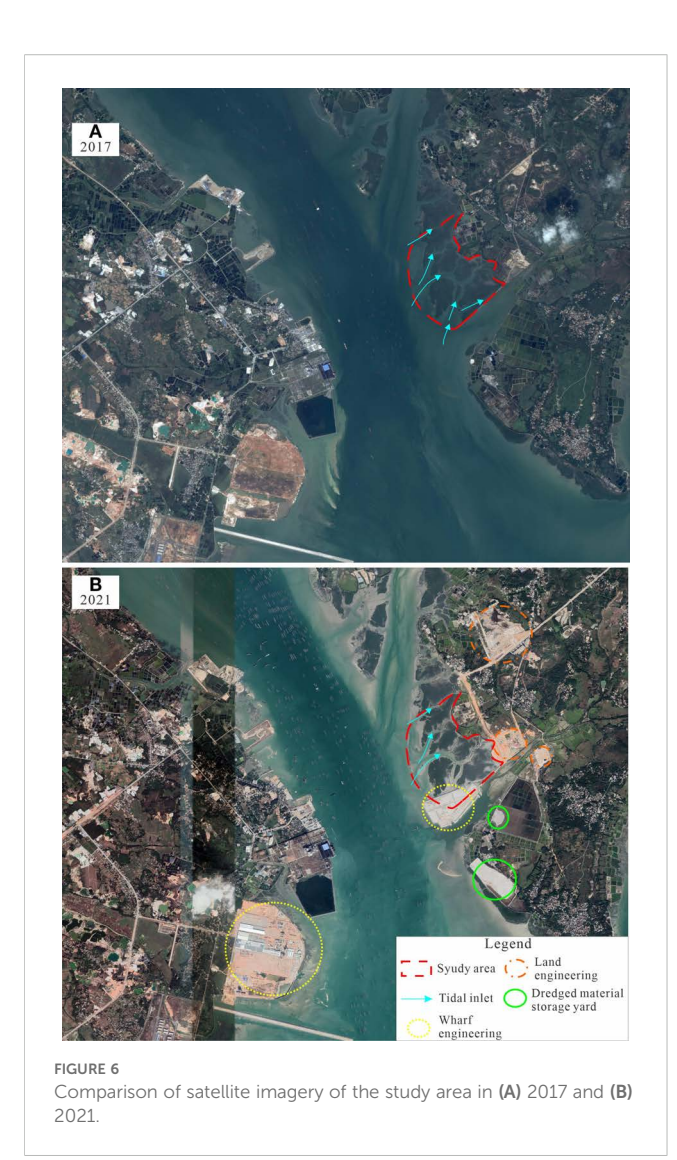


Preserved Core (B2): Topographically elevated within the mangrove matrix.

Degraded Zones (A1-A3): Situated in microrelief depressions. Degraded Fringe (A4): proximal to active construction zones.

Topographic positioning prolongs inundation duration in degraded zones. Fine-grained sediments flocculate into suspensions, undergoing tidal advection and preferential deposition. Subsequent kaolinite enrichment exploits colloidal properties (granulometry, expandability, cohesion), reducing sediment porosity and inducing rootzone hypoxia.

Synthesis of these mechanisms indicates that coastal engineering interventions have fundamentally modified sediment budgets and hydrodynamic regimes. The synergistic effects of increased kaolinite input pathways and decreased tidal flushing capacity have shifted Area A from a transit-dominated to a sink-dominated sedimentary environment. The synergistic interplay of topographic parameters (elevation, microrelief) and sedimentary properties (granulometry, drainage capacity) exacerbates kaolinite's functional dominance in mangrove degradation processes. This anthropogenic forcing exceeds natural variability observed in



Area B, providing a clear signature of human-mediated coastal transformation.

4.3 Ecological impacts

Kaolinite enrichment, driven by its inherent layered structure and swelling capacity, reduces sediment porosity, impedes root oxygen diffusion, and exacerbates hypoxic stress in mangrove ecosystems—a phenomenon documented in Qinzhou mangroves where coastal engineering (e.g., land reclamation, seawalls, bridge construction) altered sediment granulometry and pore architecture (Wang et al., 2025). Concurrently, increased fine-grained sediment accretion reduces aeration porosity within mangrove substrates, impairing drainage capacity and gas exchange. This leads to prolonged water retention after ebb tides, ultimately impeding pneumatophore development and root oxygenation. While controlled inundation enhances mangrove productivity (Chen et al., 2004), protracted submersion (>8 hours/tidal cycle) induces

progressive rootzone hypoxia, suppressing growth rates, diminishing leaf area, and lowering survival probabilities (Curran et al., 1986; Pezeshki et al., 1990; Hoveenden et al., 1995; Ellison and Farnswoah, 1997; Chen et al., 2004, Chen et al., 2006).

4.4 Restoration strategies

Hydrodynamic Restoration: Dredging tidal channels and reestablishing natural sediment transport pathways to leverage tidal amplitude for scouring fine-grained kaolinite deposits.

Terrestrial Input Management: Implementing sedimentation basins in dredged zones and installing filtration screens at drainage outlets to sequester suspended kaolinite, thereby mitigating terrestrial-derived kaolinite inputs.

Through science-based selection of dredging methodologies and rigorous enforcement of environmental safeguards, dual objectives of economic advancement and sustainable mangrove ecosystem conservation can be synergistically realized.

5 Conclusions

This study elucidates spatial heterogeneity in sediment mineral composition between degraded and preserved mangrove zones, demonstrating that anthropogenic activities (e.g., port construction, channel dredging) alter regional sedimentary dynamics and sediment provenance, perturbing mineral assemblages and inducing clay mineral enrichment. Such enrichment reduces sediment porosity, resulting in rootzone hypoxia that suppresses mangrove growth and ultimately triggers ecosystem degradation. Restoring hydrodynamic conditions, controlling terrestrial inputs, and implementing substrate mineral amendment can mitigate engineering-induced stresses on mangrove ecosystems.

Data availability statement

The original contributions presented in the study are included in the article/supplementary material. Further inquiries can be directed to the corresponding author.

Author contributions

LZ: Resources, Conceptualization, Validation, Methodology, Funding acquisition, Writing – review & editing, Supervision, Investigation, Writing – original draft, Formal Analysis. DC: Writing – review & editing, Methodology, Data curation, Validation, Funding acquisition, Writing – original draft, Formal Analysis. HT: Formal Analysis, Visualization, Resources, Writing – review & editing. YW: Software, Writing – review & editing. YQ: Investigation, Writing – review & editing, Visualization, Data curation. YX: Formal Analysis, Conceptualization, Supervision, Writing – review & editing.

Funding

The author(s) declare financial support was received for the research and/or publication of this article. This work was financially supported by Scientific Research Start Funds Project of the Innovation Driven Development Foundation of Guangxi (Grant No. AD22080034, AD22080035), Scientific Research Fund of the Fourth Institute of Oceanography, MNR (Grant No. 202106), the Special found for the Ministry of Natural Resources (Grant No. CB202402015, CB202501001).

Conflict of interest

The authors declare that the research was conducted in the absence of any commercial or financial relationships that could be construed as a potential conflict of interest.

References

Alongi, D. M. (2014). Carbon cycling and storage in mangrove forests. 2014. Annu. Rev. Mar. Sci 6, 195–219. doi: 10.1146/annurev-marine-010213-135020

Bunting, P., Rosenqvist, A., Hilarides, L., Lucas, R., and Thomas, N. (2022a). Global mangrove watch: updated 2010 mangrove forest extent (v2.5). *Remote Sens.* 14, 1034. doi: 10.3390/rs14041034

Bunting, P., Rosenqvist, A., Hilarides, L., Lucas, R., Thomas, N., Tadono, T., et al. (2022b). Global mangrove extent change 1996-2020: global mangrove watch version 3.0. Remote Sens. 14, 3657. doi: 10.3390/rs14153657

Chaudhuri, P., Nath, B., and Birch, G. (2014). Accumulation of trace metals in grey mangrove Avicennia marina fine nutritive roots: The role of rhizosphere processes. *Mar. pollut. Bull.* 79, 284–292. doi: 10.1016/j.marpolbul.2013.11.024

Chen, L. Z., Lin, P., and Wang, W. Q. (2006). Mechanisms of mangroves waterlogging resistance. China). *Acta Ecologica Sin.* 26, 586–593.

Chen, L. Z., Wang, W. Q., and Peng, L. (2004). P. Influence of water logging time on the growth of *Kandelia candel* seedlings. *Acta Oceanologica Sin.* 23, 149–158.

Curran, M., Cole, M., and Allaway, W. G. (1986). Root aeration and respiration in young mangrove plants (Avicennia marina (Forsk.) Vierh). *J. Exp. Bot.* 37, 1225–1233. doi: 10.1093/jxb/37.8.1225

Ellison, A. M., and Farnswoah, E. J. (1997). Simulated sea level change alters anatomy, physiology, growth, and reproduction of red mangrove (Rhizophora mangle L.). *Oecologia* 112, 435–446. doi: 10.1007/s004420050330

Ellison, A. M., Farnsworth, E. J., and Merkt, R. E. (1999). Origins of mangrove ecosystems and the mangrove biodiversity anomaly. *Global Ecol. Biogeography* 8, 95–115. doi: 10.1046/j.1466-822X.1999.00126.x

Gilman, E. L., Ellison, J., Duke, N. C., and Field, C. (2008). Threats to mangroves from climate change and adaptation options: a review. *Aquat. Bot.* 89, 237–250. doi: 10.1016/j.aquabot.2007.12.009

Goldberg, L., Lagomasino, D., Thomas, N., and Fatoyinbo, T. (2020). Global declines in human-driven mangrove loss. *Global Change Biol.* 26, 5844–5855. doi: 10.1111/gcb.15275

Grellier, S., Janeau, J. L., Nhon, D. H., Cuc, N. T. K., Quynh, L. T. P., Thao, P. T. T., et al. (2017). Changes in soil characteristics and C dynamics after mangrove clearing (Vietnam). *Sci Total Environ*. 593-594, 654–663. doi: 10.1016/j.scitotenv.2017.03.204

Hamilton, S. E., and Casey, D. (2016). Creation of a high spatio-temporal resolution global database of continuous mangrove forest cover for the 21st century (CGMFC-21). *Global Ecol. biogeography* 25, 729–738. doi: 10.1111/geb.12449

Hoveeden, M. J., Curran, M., Cole, M. A., Gouher, P. F. E., Skelton, N. J., and Allaway, W. G. (1995). Ventilation and respiration in roots of one-year-old seedlings of grey mangrove Avicennia marina (Forsk.) Vierh. *Hydrobiologia* 295, 23–29. doi: 10.1007/BF00029107

Li, X. H., Zhou, H. W., Liu, Y., Lee, C., Sun, M., Chen, C. H., et al. (2000). Shoshonitic intrusive suite in SE Guangxi: Petrology and geochemistry. *Chinese Science Bulletin* 45, 653–659. doi: 10.1007/BF02886045

Liao, B. W., and Zhang, Q. M. (2014). Area, distribution and species composition of mangroves in China. *Wetland Sci* 12, 435-440. doi: 10.13248/j.cnki.wetlandsci.2014.04.005

Generative AI statement

The author(s) declare that no Generative AI was used in the creation of this manuscript.

Any alternative text (alt text) provided alongside figures in this article has been generated by Frontiers with the support of artificial intelligence and reasonable efforts have been made to ensure accuracy, including review by the authors wherever possible. If you identify any issues, please contact us.

Publisher's note

All claims expressed in this article are solely those of the authors and do not necessarily represent those of their affiliated organizations, or those of the publisher, the editors and the reviewers. Any product that may be evaluated in this article, or claim that may be made by its manufacturer, is not guaranteed or endorsed by the publisher.

Meng, W., Zhai, S. J., Qin, Y. W., and Zhang, B. H. (2006). Sources identification of heavy metals in core sediments of bohai bay. *Mar. Sci Bull.* 25, 62–69.

Numbere, A. O., and Obanye, C. J. (2023). Environmental impact of bush burning on the physico-chemistry of mangrove soil at eagle island, Niger delta, Nigeria. *Am. J. Plant Sci.* 14, 191–201. doi: 10.4236/ajps.2023.142015

Pezeshki, S. R., Delaune, R. D., and Patrick, W. H. Jr (1990). Differential response of selected mangroves to soil flooding and salinity: gas exchanges and biomass partitioning. *Can. J. For. Res.* 20, 869–874．.

Qin, X. F., Pan, Y. Y. M., Li, J., Li, R. S., Zhou, F. S., Hu, G. A., et al. (2006). Zircon SHRIMP U-Pb geochronology of the Yunkai metamorphic complex in southeastern Guangxi, China. *Geological Bull. China* 25, 553–559.

Rezaei, M., Kafaei, R., Mahmoodi, M., Sanati, A. M., Vakilabadi, D. R., Arfaeinia, H., et al. (2021). Heavy metals concentration in mangrove tissues and associated sediments and seawater from the north coast of Persian Gulf, Iran: Ecological and health risk assessment. *Environ. Nanotechnology Monit. Manage.* 15, 100456. doi: 10.1016/j.emmm.2021.100456

Souza, I. D. C., Rocha, L. D., Morozesk, M., Bonomo, M. M., Arrivabene, H. P., Duarte, I. D., et al. (2015). Changes in bioaccumulation and translocation patterns between root and leafs of Avicennia schaueriana as adaptive response to different levels of metals in mangrove system. *Mar. pollut. Bull.* 94, 176–184. doi: 10.1016/j.marpolbul.2015.02.032

Spalding, M., Kainuma, M., and Collins, L. (2010). World atlas of mangroves (London, UK: Earthscan), 1–336.

Temmerman, S., Meire, P., Bouma, T. J., Herman, P. M. J., Ysebaert, T., and De Vriend, H. J. (2013). Ecosystem-based coastal defence in the face of global change. *Nature* 504, 79–83. doi: 10.1038/nature12859

United Nations Environment Programme (UNEP) (2014). *The importance of mangroves to people: a call to action*. Eds. J. van Bochove, E. Sullivan and T. Nakamura (Cambridge: UNEP World Conservation Monitoring Centre).

Usman, A. R. A., Alkredaa, R. S., and Al-Wabel, M. I. (2013). Heavy metal contamination in sediments and mangroves from the coast of Red Sea: Avicennia marina as potential metal bioaccumulator. *Ecotoxicology Environ. Saf.* 97, 263–270. doi: 10.1016/j.ecoenv.2013.08.009

Wang, R. M., Dai, Z. J., Wu, T. L., Huang, H., Ou, Y. N., and Zhou, T. S. (2025). Study on dynamic changes of mangrove spatial distribution in jingujiang river, guangxi. *Advance Mar. Sci* 43, 1–14. doi: 10.12362/j.issn.1671-6647.20231123001

Wang, Q., Ma, L., Huang, K. J., Lei, Z. Y., and Xie, S. Y. (2021). Quantitative analysis of kaolinite, illite and montmorillonite by X - ray diffraction. *Guizhou Geology* 38, 71–78.

Xia, P. (2011). Variation of Sediment environment quality under the influence of human activities and its impact on the mangrove development over the past 100 years in the coastal zone of Guangxi province. Ph.D. Dissertation (Qingdao: Ocean University of China), 1–118.

Xia, X. M. (2015). Hannansheng haiyang ziyuan Huanjing zhuangkuang (Beijing: China Ocean Press), 1–788.

Zhang, J. F., Gan, S. C., Yang, P. J., Zhou, J. G., Huang, X. Y., Chen, H., et al. (2024). A global assessment of mangrove soil organic carbon sources and implications for blue carbon credit. *Nat. Commun.* 15, 8994. doi: 10.1038/s41467-024-53413-z

Zhang, T., Hu, S. S., He, Y., You, S. C., Yang, X. M., Gan, Y. H., et al. (2021). A fine-scale mangrove map of China derived from 2-meter resolution satellite observations and field data. *ISPRS Int. J. Geo-Information* 10, 92. doi: 10.3390/ijgi10020092

Zhang, X. B., Wang, M. F., Pi, D. H., Liu, K., Guo, X. N., and Wang, Y. B. (2017). Ar-Ar geochronology of muscovite and metallogenic geodynamics of Xinhua Pb-Zn (Ag) deposit in Yunkai area, Guangxi. *Mineral Deposits* 36, 979–991. doi: 10.16111/j.0258-7106.2017.04.012

Zhao, Y. S., Zhou, Y., Xu, C., Cai, Y. F., Han, Z. X., Fang, G. C., et al. (2023). Geochemical characteristics and rare earth metallogenic indication of Yanshanian granite in Southeast Guangxi. *Chin. J. Geology* 58, 890–909. doi: 10.12017/dzkx.2023.049